Frontiers in Heat and Mass Transfer

Tech Science Press

DOI: 10.32604/fhmt.2023.041793

ARTICLE

Analysis of Profile and Unsteady Flow Performance of Variable Base Circle Radius Scroll Expander

Junying Wei*, Gang Li, Chenrui Zhang, Wenwen Chang and Jidai Wang

College of Mechanical and Electronic Engineering, Shandong University of Science and Technology, Qingdao, 266590, China

*Corresponding Author: Junying Wei. Email: jdwjy0726@163.com

Received: 06 May 2023 Accepted: 19 July 2023 Published: 30 November 2023

ABSTRACT

To study the complex internal flow field variation and output characteristics of a variable base radius scroll expander, this paper uses dynamic mesh techniques and computational fluid dynamics (CFD) methods to perform transient numerical simulations of a variable base radius scroll expander. Analysis of the flow field in the working cavity of a variable base radius scroll expander at different spindle angles and the effect of different profiles, speeds and pressures on the output characteristics of the scroll expander. The results of the study show that due to the periodic blocking of the inlet by the orbiting scroll, the fluid hits the internal walls of the expander at different flow rates, with excessive mechanical losses, resulting in an uneven distribution of the internal flow field. At the same temperature, pressure and scroll plate diameter, the variable base radius scroll expander increases the output torque by 0.046 N·m, the output power by 9.634 W and the isentropic efficiency by 3.8% compared to the fixed base circle scroll expander. As the speed is inversely proportional to the output torque, the isentropic efficiency of the expander tends to increase and then decrease as the speed increases. The density of the fluid is directly proportional to the pressure over a range of pressures. As the pressure increases from 0.6 to 0.9 Mpa, the average mass flow rate and isentropic efficiency increase by 0.02357 kg/s, and 6.61%, respectively.

KEYWORDS

Scroll expander; variable base circle radius; internal flow field; output characteristics

Nomenclature

r_b	The initial radius of the base circle (mm)
k	Radius coefficient
h	Height of scroll teeth (mm)
R_{or}	The radius of gyration (mm)
N	Scroll turns
f, i	The inner side of the fixed scroll
d, i	The inner side of orbiting scroll
f, o	The outer side of the fixed scroll
d, o	The outer side of orbiting scroll
q_m	The mass flow rate of a fluid (kg/s)

$\overline{T}$	The average value of torque (N·m)
h_{in}	Inlet Enthalpy
h_{out}	Outlet Enthalpy
h_{sout}	entropy-enthalpy ratio
F_t	Tangential gas forces (N)
F_r	Radial gas forces (N)
F_a	Axial gas forces (N)

e.g.

α	The angle of involute occurrence (rad)
φ_e	Involute terminal angle (rad)
ϕ	The corrected angle of expansion (rad)
γ	Correction angle (rad)
λ	Effective area factor (rad)

1 Introduction

As a key component of a micro-compressed air energy storage system (CAES), the scroll expander has been the focus of much scholarly attention due to its simple structure, stable operation, and excellent isentropic efficiency [1–3]. Many studies have simulated the internal flow field of scroll expanders by using thermodynamic models or employing CFD methods to investigate changes in the interior flow field of scroll expanders to enhance scroll expander output characteristics [4].

Liu et al. [5] developed a three-dimensional (3D) transient numerical model of a scroll expander to investigate the connection between the external expansion ratio and the transient driving torque of the expander under the same exhaust pressure. The results show that the higher the external expansion ratio, the higher the outlet mass flow rate and transient output torque of the expander. Peng et al. [6] developed two mathematical models of the equal and varying cross-section to investigate the variation of a scroll expander's fluid field with spindle angle. The results show that the variable section has less internal leakage, higher output, and superior overall performance compared to the equal section expander. Yang et al. [7] used CFD methods and dynamic mesh techniques to numerically simulate a two-dimensional (2D) scroll expander. The results show that the pressure and velocity distribution of the scroll expander is not uniform. Liu et al. [8] developed a 3D transient model of the expander to show the fluctuation of the expander's internal flow field with spindle angle at various suction temperatures. The results reveal that the axial gas force in the orbiting scroll is inversely proportional to the suction temperature, but the radial and tangential gas forces are proportional. Emhardt et al. [9] performed non-stationary numerical simulations of a variable wall thickness scroll expander to determine the expander's aerodynamic performance at various pressure ratios. Studies have shown that under-expansion and over-expansion occur in expanders at high and low pressure ratios respectively. The high-pressure ratio leads to increased radial clearance in the expander, resulting in severe internal leakage. Song et al. [10] used CFD to model a scroll expander that had two exhaust designs and analyzed the circling scroll output characteristics under the two exhaust configurations. The results show that the symmetrical exhaust structure has a greater variation in exhaust mass flow rate but a more even flow distribution between the exhaust and back pressure cavities, increasing the output torque of the expander. Feng et al. [11] created a 3D transient model of a small ORC scroll expander to investigate the effect of critical factors on the scroll expander's performance and to find the best

RSM solution. According to research, the unequal velocity distribution in the asymmetrical working cavity results in variable flow velocities in the suction cavity at the orbiting and fixed scroll walls. For the performance of scroll expanders, pressure loads have a greater influence than temperature loads. Sun et al. [12] used CFD methods to validate the thermodynamic model accuracy of an oil-free scroll expander and to analyze the flow and distribution patterns of the working cavity and exhaust pipe. The study found that the pressure in the suction cavity is an important component of the expander's output efficiency. The flow field is not equally distributed throughout the expander's working cavity, and there is substantial fluid leakage into the next working cavity, with the majority of the gas going into the exhaust port via the deformation zone. Wei et al. [13] modeled a scroll expander for an ORC waste heat recovery system and carried out 3D non-constant CFD simulations to analyze the vortex flow properties of the suction and expansion cavities in the scroll expander. The results reveal that the orbiting scroll tooth head's obstructive impact causes a continual shift in the position and amount of pressure distortion at the suction port outlet.

In this paper, we first establish the fluid domain model inside the variable base circle scroll expander and use the dynamic mesh technique and CFD method to study the flow field change law inside the scroll expander with the variable base circle. Then, the changes in gas force and isentropic efficiency are compared separately for the variable base circular profile, the fixed base circular profile, and the combined higher order profile. Finally, the fluctuation of the isentropic efficiency of the variable base circle scroll expander at different speeds and pressures is analyzed.

2 Mathematical Models

2.1 Geometric Models

From the fixed base circle radius involute equation and the conjugate curve meshing condition, the equation of the inner and outer profile of the orbiting and the fixed scroll of the variable base circle scroll expander can be derived [14]. The equation for the fixed scroll disc type line is Eqs. (1) and (2) and the equation for the orbiting scroll type line is Eqs. (3) and (4), respectively. As the scroll profile interferes with the tool during machining causing overcutting, a head correction is required for the orbiting and fixed scroll profile [15,16]. In this paper, a double circular arc plus straight line correction method is used for the correction. The specific design parameters of the orbiting and fixed scroll are shown in Table 1.

$$\begin{cases} x_{f,o} = (r_b + k\varphi)\cos\varphi + \left(r_b\varphi + \frac{k}{2}\varphi^2\right)\sin\varphi \\ y_{f,o} = (r_b + k\varphi)\sin\varphi - \left(r_b\varphi + \frac{k}{2}\varphi^2\right)\cos\varphi \end{cases} \tag{1}$$

$$\begin{cases} x_{f,i} = (r_b + k\varphi)\cos(\varphi + \pi) + \left[r_b(\varphi + \pi - \alpha) + \frac{k}{2}\left(\varphi^2 - (\alpha - \pi)^2\right)\right]\sin(\varphi + \pi) \\ y_{f,i} = (r_b + k\varphi)\sin(\varphi + \pi) - \left[r_b(\varphi + \pi - \alpha) + \frac{k}{2}\left(\varphi^2 - (\alpha - \pi)^2\right)\right]\cos(\varphi + \pi) \end{cases} \tag{2}$$

$$\begin{cases} x_{d,i} = -(r_b + k\varphi)\cos(\varphi + \pi) - \left[r_b(\varphi + \pi - \alpha) + \frac{k}{2}\left(\varphi^2 - (\alpha - \pi)^2\right)\right]\sin(\varphi + \pi) + R_{or}\cos\theta \\ y_{d,i} = -(r_b + k\varphi)\sin(\varphi + \pi) + \left[r_b(\varphi + \pi - \alpha) + \frac{k}{2}\left(\varphi^2 - (\alpha - \pi)^2\right)\right]\cos(\varphi + \pi) + R_{or}\sin\theta \end{cases} \tag{3}$$

$$\begin{cases} x_{d,o} = -x_{f,o} + R_{or}\cos\theta \\ y_{d,o} = -y_{f,o} + R_{or}\sin\theta \end{cases} \tag{4}$$

Table 1: The specific design parameters of the orbiting and fixed scroll

The basic parameters	The parameter value
The initial radius of the base circle	3.5
Radius coefficient	−0.07
The angle of involute occurrence	0.72
Scroll body wall thickness	2∼8
Height of scroll teeth	33.5
The radius of gyration	5.854
Involute terminal angle	5.2π
Scroll turns	2.35
The corrected angle of expansion	0.56π
Correction angle	0.32π

As shown in Fig. 1, the wall thickness of the scroll tooth is the largest in the central part and the smallest in the outermost part, which can improve the stress condition of the central part and obtain better strength and stiffness [17]. Compared with the scroll tooth with equal wall thickness, its adaptive operating pressure is increased.

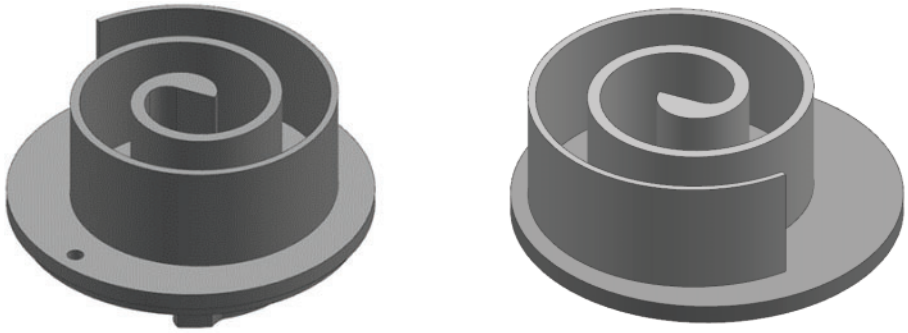

(a) Fixed scroll (b) Orbiting scroll

Figure 1: The 3D structure of the orbiting and fixed scroll

2.2 Numerical Models

2.2.1 Mesh Generation

The working cavity and the inlet and exhaust calculation domains have meshed separately in the Mesh module of Workbench. The fluid domain of the working cavity is meshed in multiple zones, and the triangular surface mesh is stretched into a trigonal mesh to ensure the quality of the mesh [18,19]. Hexahedral meshing is applied to the fluid domain of the inlet and outlet to improve the accuracy and speed of computation, and an interface is set at the intersection with the fluid domain of the working cavity. The result and number of meshing are 1567767, as shown in Fig. 2.

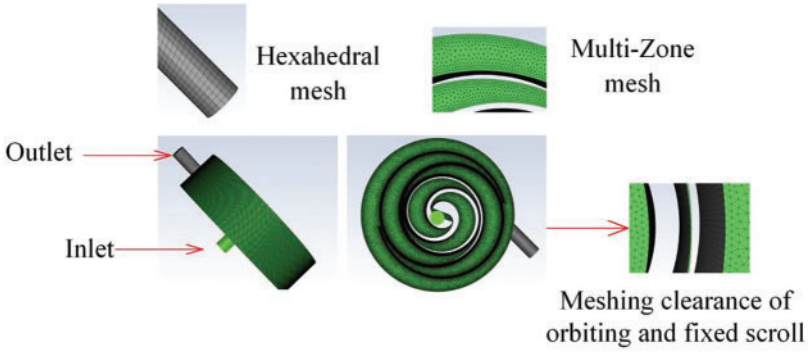

Figure 2: Fluid calculation domain meshing

2.2.2 Parameter Settings

The simulated boundary conditions are as follows:

1. The boundary conditions are pressure-inlet and pressure-outlet. The inlet pressure is 0.6 MPa, and the outlet pressure is atmospheric.
2. The fluid medium selected is ideal air.
3. Open the energy equation, the RNG $k-\varepsilon$ model was selected for the physical model setting, and near-wall treatment was adopted.
4. Since the PISO algorithm can effectively weaken the influence of mesh distortion on the convergence of calculation, this paper uses the PISO algorithm to simulate and solve the transient state of the scroll expander [20]. This algorithm is adopted because it can recalculate the pressure correction gradient at each step. To accelerate the convergence of results and ensure the quality of the mesh, the second-order upwind scheme is adopted in the spatial dispersion except for the Least Squares Cell Based on the gradient.
5. The DEFINE_GRID_MOTION macro command in the user-defined function of Fluent is used to realize counterclockwise translation of the orbiting scroll around the fixed scroll.
6. The dynamic grid adapts spring smoothing, 2.5D plane reconstruction, and local plane reconstruction. In the dynamic grid area, the orbiting scroll plate area is set as a rigid body, the upper and lower surfaces of the working cavity are set as a deformation area, and other areas are set as static areas [21,22].

3 Unsteady Flow Field Analysis

3.1 Pressure Field Analysis

The pressure field distribution of a variable base circle radius scroll expander at different spindle angle positions is shown in Fig. 3. When the spindle angle of rotation is $\pi/2$, the orbiting scroll does not shade the air inlet, resulting in a more uniform pressure distribution and a lower degree of asymmetry in the symmetrical working cavity. The pressure from the central suction cavity to the exhaust cavity decreases from high to low. When the spindle angle of rotation is π, the high-pressure air continues to enter the suction cavity through the air inlet, and the orbiting scroll plate tooth head begins to obscure the air inlet, resulting in uneven pressure distribution in the expansion cavity. When the spindle angle of rotation is $3\pi/2$, the scroll expander suction is complete. Due to the shielding effect of the orbiting scroll on the air inlet, the high-pressure air does not flow into the suction cavity equally, which leads to

the uneven pressure distribution in the suction cavity that the degree of asymmetry increases. When the spindle angle of rotation is 2π, the scroll expander begins to inhale, and the gas in the expansion cavity expands. The swirling flow in the working cavity and the eccentric rotating motion of the orbiting scroll result in an unequal distribution of pressure in the suction and expansion cavities.

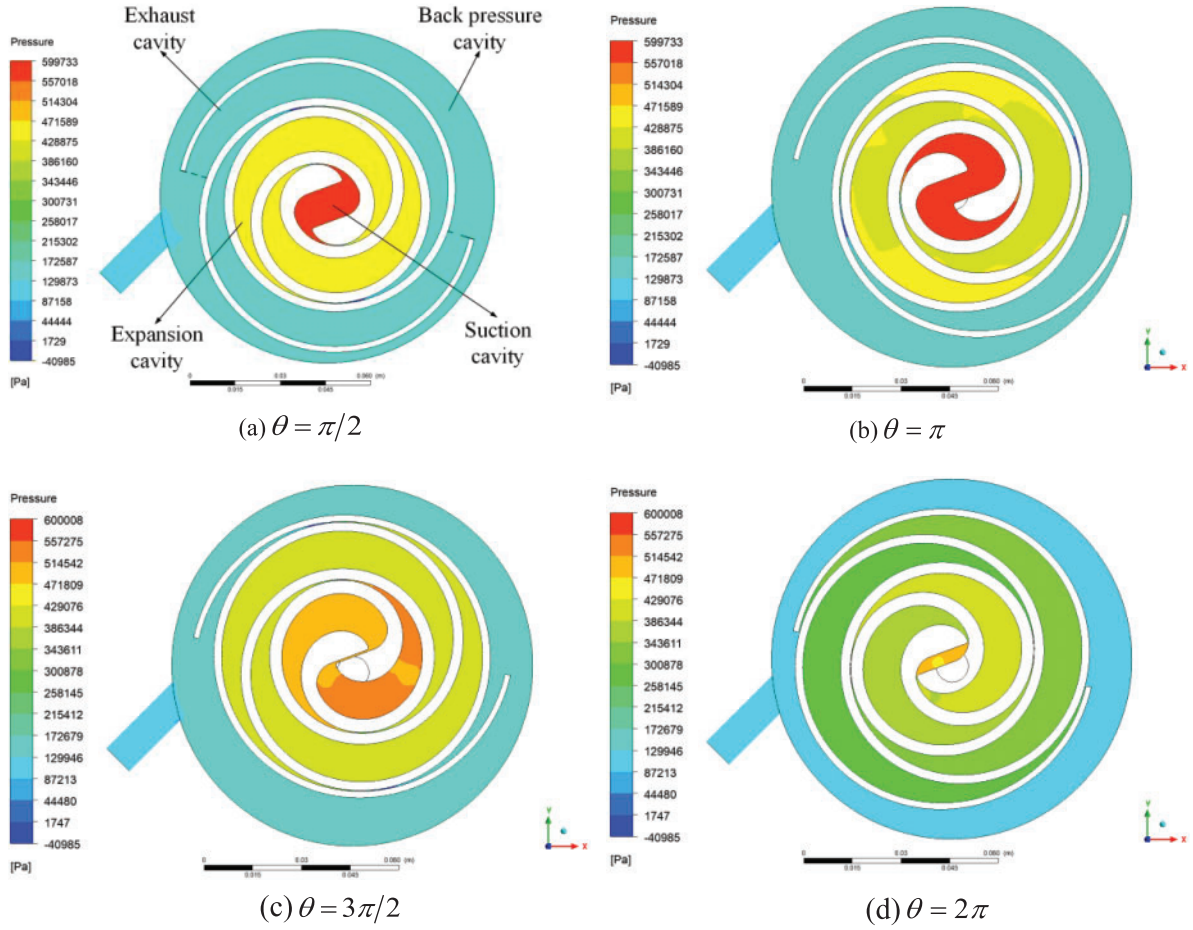

Figure 3: Pressure field distribution of scroll expander

3.2 Velocity Field Analysis

The velocity field distribution of a variable base circle radius scroll expander at different spindle angle positions is shown in Fig. 4. When the spindle angle of rotation is $\pi/2$, the air inlet is completely opened and the orbiting scroll has no shelter for it. Therefore, the distribution of gas flow velocity is uniform and the degree of asymmetry is small. When the spindle angle of rotation is π, the orbiting scroll can block the air inlet. The uneven distribution of gas velocity is increased because of the existence of swirling flow in the working cavity. The maximum speed is 548 m/s at the meshing clearance. When the spindle angle of rotation is $3\pi/2$, the phenomenon of swirling flow caused by throttling and wall obstruction increases. As a result, the uneven distribution of gas flow velocity becomes more obvious. When the spindle angle of rotation is 2π, the scroll expander begins to inhale that the air inlet is gradually opened, the phenomenon of swirling flow in the working cavity is reduced and the unevenness of gas flow velocity distribution is reduced.

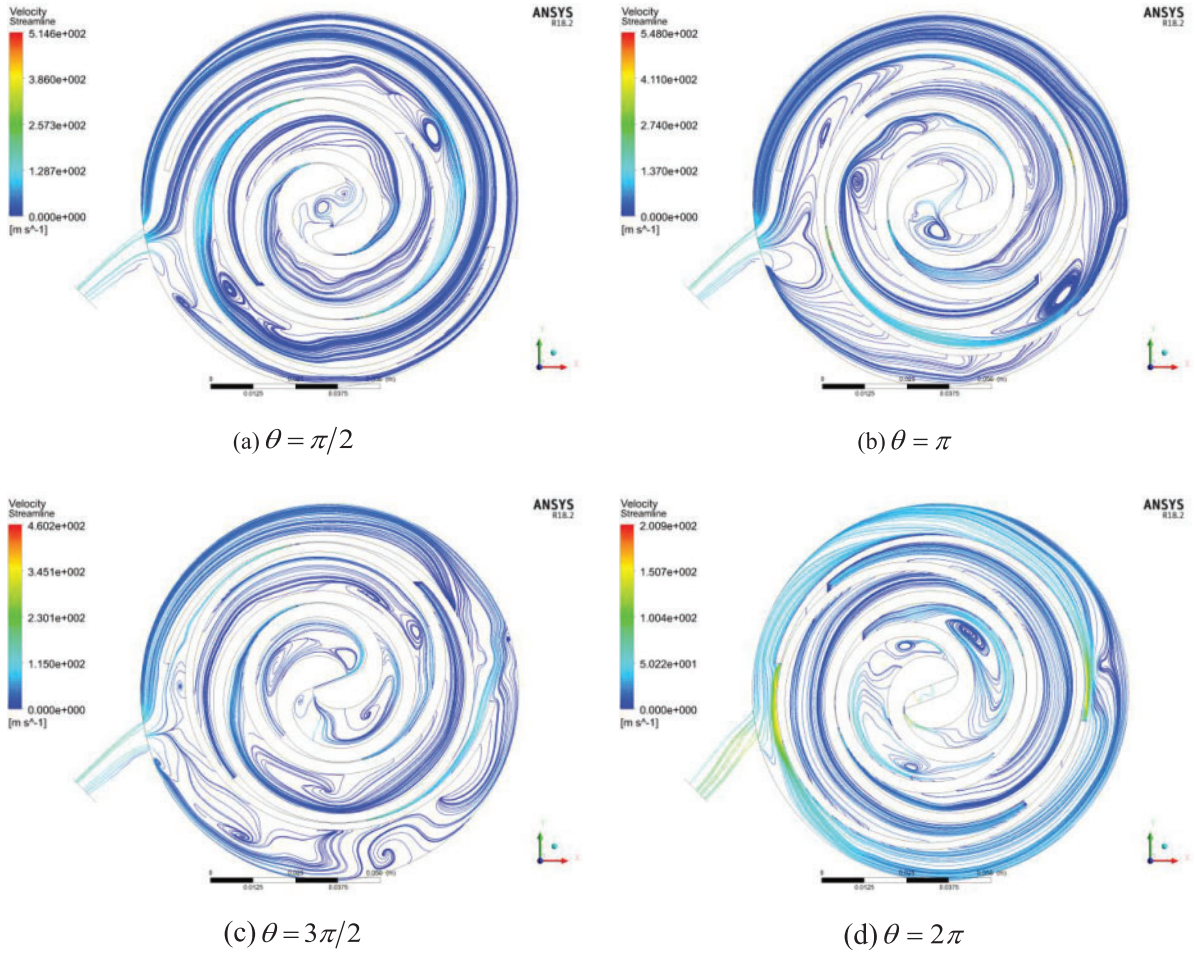

(a) $\theta = \pi/2$ (b) $\theta = \pi$

(c) $\theta = 3\pi/2$ (d) $\theta = 2\pi$

Figure 4: Velocity streamline diagram of scroll expander

3.3 Temperature Field Analysis

The temperature field distribution of a variable base circle radius scroll expander at different spindle angle positions is shown in Fig. 5. When the spindle angle of rotation is $\pi/2$, the temperature of the suction cavity is highest. The temperature of the fluid in the expansion cavity near the suction cavity is higher due to the squeezing effect of the orbiting scroll teeth, while the temperature of the fluid near the exhaust cavity decreases under the expansion effect. Due to the high velocity of the mass hitting the wall of the scroll plate during the exhaust process a high gas pulsation is generated, resulting in a higher local temperature in the back pressure cavity than in the exhaust cavity. When the spindle angle of rotation is π, the degree of asymmetry of temperature field distribution decreases. Because of the swirling flow in the working cavity, mechanical dissipation raises the temperature in the working cavity. When the spindle angle of rotation is $3\pi/2$, the temperature of the suction cavity fluctuates, with the temperature of the suction cavity near the inlet side being greater than the temperature of the symmetrical suction cavity. When the spindle angle of rotation is 2π, the temperature asymmetry distribution is obvious that the overall temperature distribution gradually decreases from the suction cavity outward. Due to the blocking of the inlet port by the tooth head, the fluid enters the suction cavity in the form of swirl flow under the larger flow resistance, and the incoming mass hits the end

plate of the orbiting scroll along the axial direction of the suction cavity, so that the mass flow rate drops rapidly as well as forming a local high-temperature zone in the working cavity, and its axial temperature distribution rises non-uniformly.

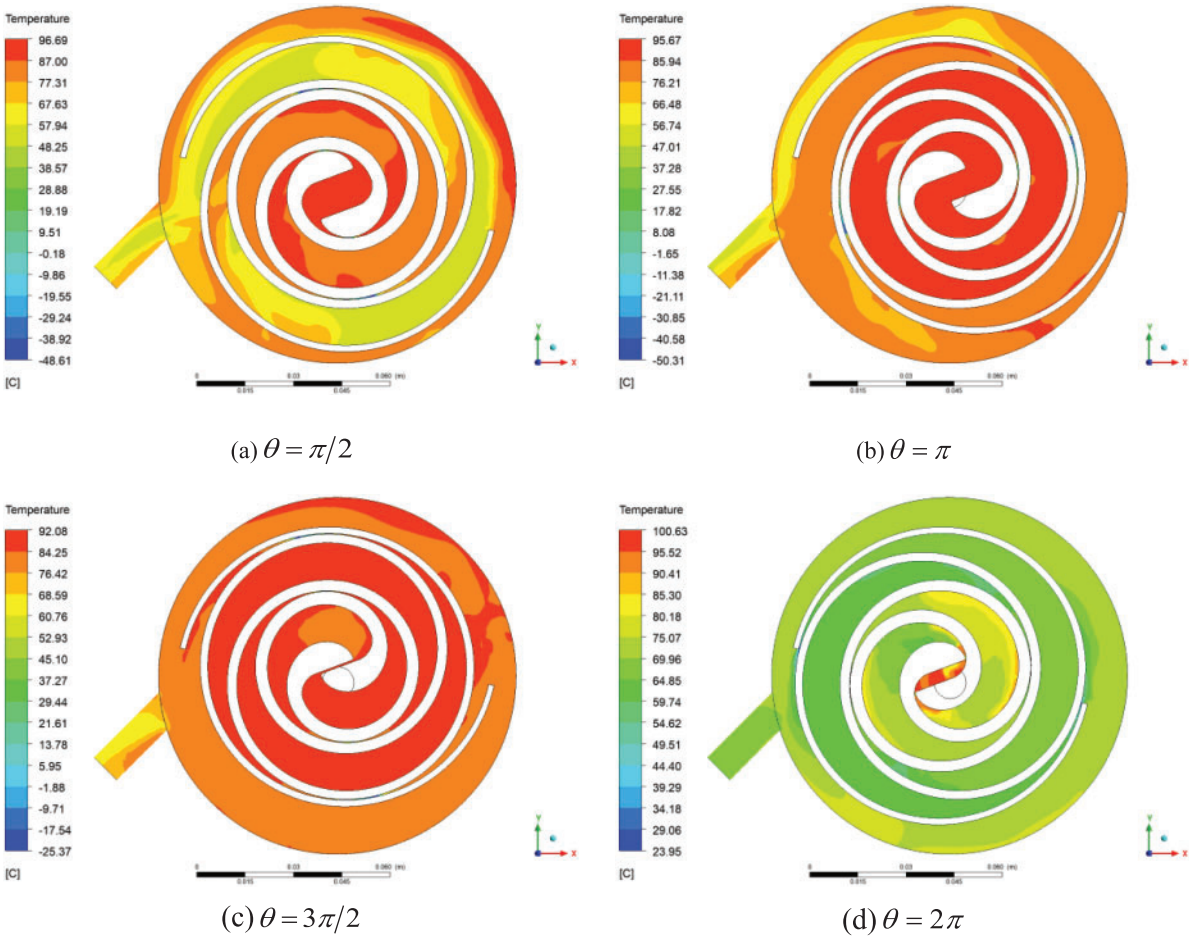

(a) $\theta = \pi/2$ (b) $\theta = \pi$

(c) $\theta = 3\pi/2$ (d) $\theta = 2\pi$

Figure 5: Temperature field distribution of scroll expander

4 Unsteady State Performance Analysis

4.1 Evaluation Indicators for the Output Characteristics of Scroll Expanders

The scroll expander's performance is primarily measured in terms of gas force, output torque, output power, and isentropic efficiency, with the last being the most important indication [23,24]. The significance of the isentropic efficiency lies in the degree of perfection of the expansion process of the fluid in the expander, and the size is equal to the ratio of the actual enthalpy drop to the enthalpy drop of the isentropic process [25,26]. The tangential pressure differential in each expansion cavity causes the amount of the scroll expander's output moment, which is equal to the difference between the tangential torque and the frictional torque [27,28]. The output torque, output power, isentropic efficiency, and average torque of a scroll expander can be calculated using Eqs. (5)–(8) [29]. As shown

in Fig. 6, the orbiting and fixed scroll discs are mainly subjected to radial gas forces, tangential gas forces, and axial gas forces [30,31].

$$T = F_t \cdot R_{\text{or}} \tag{5}$$

$$P = T \cdot \omega = T \cdot \frac{2\pi n}{60} \tag{6}$$

$$\overline{T} = \int_0^{2\pi} T(\theta)\, d\theta \tag{7}$$

$$\eta = \frac{h_{in} - h_{out}}{h_{in} - h_{sout}} = \frac{P}{q_m (h_{in} - h_{out})} \tag{8}$$

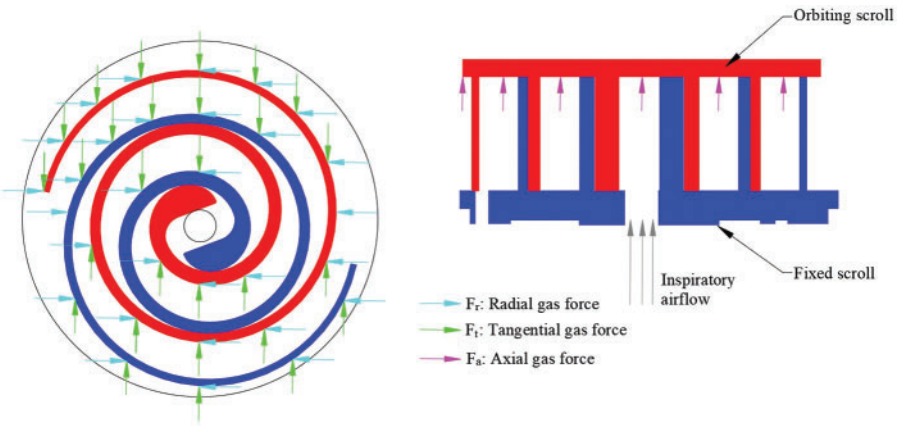

Figure 6: Schematic diagram of gas forces in orbiting and fixed scroll

4.2 Effect of Different Scroll Profiles on Scroll Expander Performance

Using compressed air as the fluid mass, the scroll profile is a fixed base circle profile, a variable base circle profile, and a combined high sub-curve profile, as shown in Table 2. Study of transient gas forces, output torque, and output power as a function of spindle rotation angle for expanders with different type lines. As can be seen in Fig. 7, the orbiting scroll tooth head shades the inlet orifice periodically as the fluid enters through the inlet, causing large fluctuations in gas forces. The combined high sub-curve has fewer scroll turns compared to the fixed and variable base circles, and the scroll plate has a smaller force area, so its axial forces are much smaller compared to the other two profiles. As the suction high-pressure gas continuously enters the suction cavity, the temperature of the suction cavity rises, the air density decreases, the leakage flow decreases, the pressure difference between the two adjacent working cavities increases, and the tangential and radial gas forces acting on the orbiting scroll increase.

As can be seen in Table 3, the variable base circle scroll expander has an increased output torque of 0.046 N·m, an increased output power of 9.634 W, and an increased isentropic efficiency of 3.8% compared to the fixed base circle scroll expander, while ensuring that the overall dimensions of the expander remain unchanged. The combination of high sub-curves with fewer scroll turns for the same scroll plate diameter results in lower volumes, so that their output torque, output power, and efficiency are lower than those of fixed base circular scroll expanders.

Table 2: Parameter settings for different scroll profiles

Parameter name	Fixed base circle (FBC)	Variable base circle (VBC)	Combined high sub-curve (CHSC)
Inlet pressure (Mpa)	0.8	0.8	0.8
Exhaust pressure (Mpa)	0.1	0.1	0.1
Inlet temperature (K)	400	400	400
Scroll plate diameter (mm)	113	113	113
Scroll turns	2.35	2.35	2

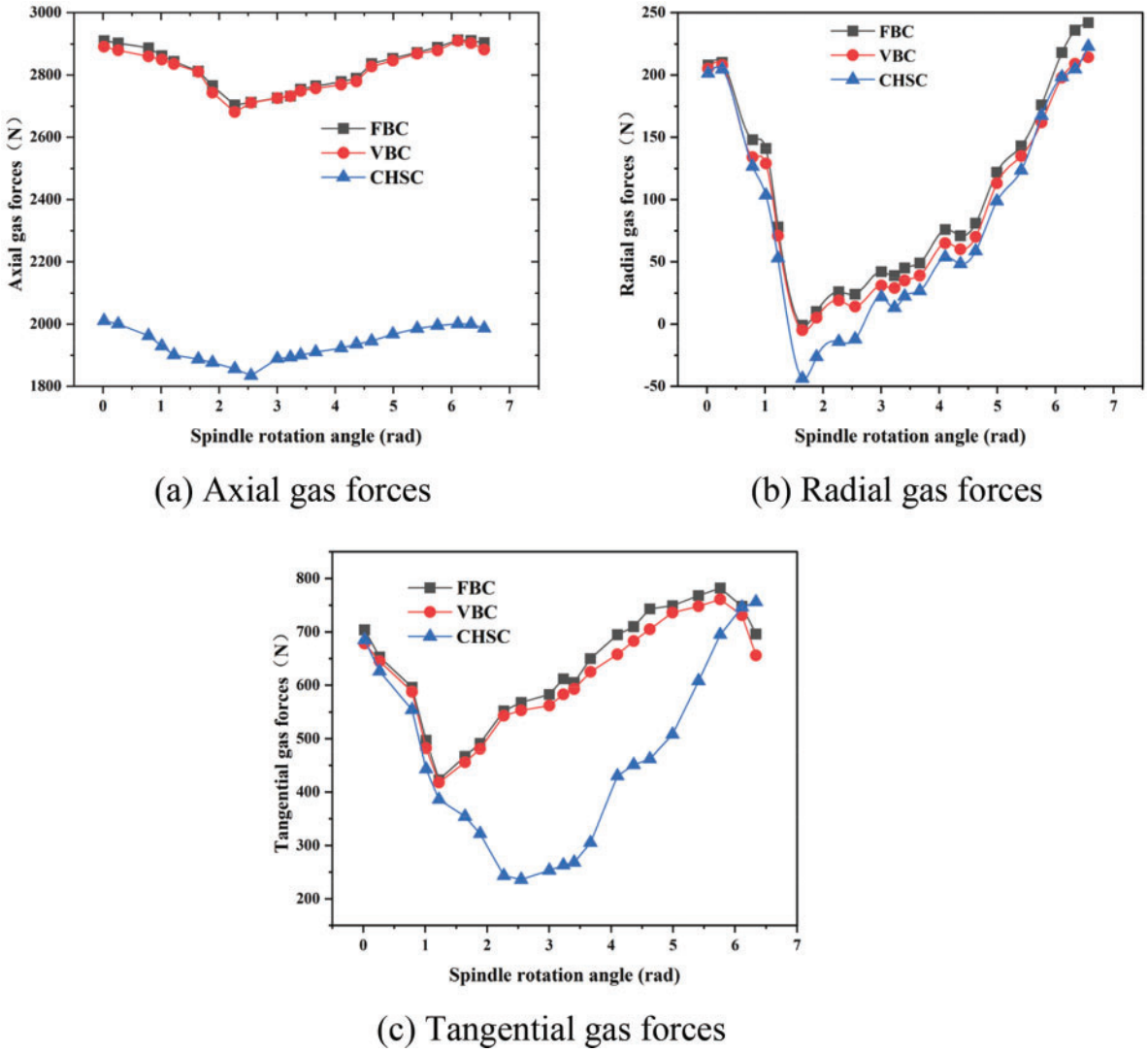

Figure 7: Transient gas force variations in the scroll expander

Table 3: Performance comparison of scroll expanders of different configurations

Scroll profile types	Output torque (N·m)	Output power (W)	Isentropic efficiency
FBC	3.265	683.820	0.419
VBC	3.311	693.454	0.457
CHSC	2.567	537.631	0.316

4.3 Effect of Different Speeds on Expander Performance

As shown in Table 4, different rotational speeds are set to study the variation of the expander's inlet mass flow rate, output torque, and output power with spindle angle at various rotational speeds. As can be seen in Fig. 8, when the expander inlet pressure and temperature remain constant, the scroll expander with the speed increase inlet flow rate is increasing, which is due to a certain inlet area, the scroll expander speed increase will accelerate the flow rate of the mass, while the relative change in gas density is not significant, increasing the flow rate of the mass. When the speed goes up from 1500 to 3000 rpm, the average flow velocity rises from 0.05396 to 0.08994 kg/s in one cycle. As the orbiting scroll rotates flat around the base circle of the fixed scroll, the orbiting scroll rotates in such a way that it blocks the air inlet, thus creating a throttling phenomenon that makes the inlet flow fluctuate widely within the same cycle.

Table 4: Different rotational speed parameter settings

Working conditions	Inlet pressure (Mpa)	Inlet temperature (K)	Outlet pressure (Mpa)	Rotational speed (rpm)
C1	0.8	400	0.1	1500
C2	0.8	400	0.1	2000
C3	0.8	400	0.1	2500
C4	0.8	400	0.1	3000

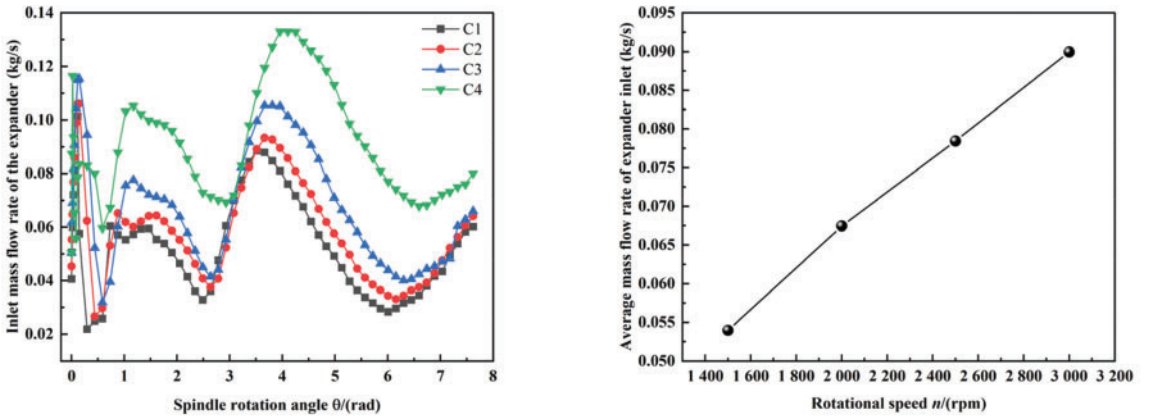

(a) Variation of inlet mass flow rate with spindle for scroll expanders at different speeds

(b) Scroll expander inlet average flow rate with speed

Figure 8: Scroll expander inlet flow *vs*. speed

When the expander's input and exit pressures are maintained constant, as shown in Fig. 9, the output torque falls as the expander speed rises. The output power of the expander is mainly influenced by the speed and output torque together, with the speed increasing, the output power gradually increases, but the output torque is inversely proportional to the speed. The output power starts to decrease under the action of the output torque, the overall trend is first increasing and then decreasing. The expander's isentropic efficiency rose by 2.69% when the speed was increased from 1500 to 3000 rpm.

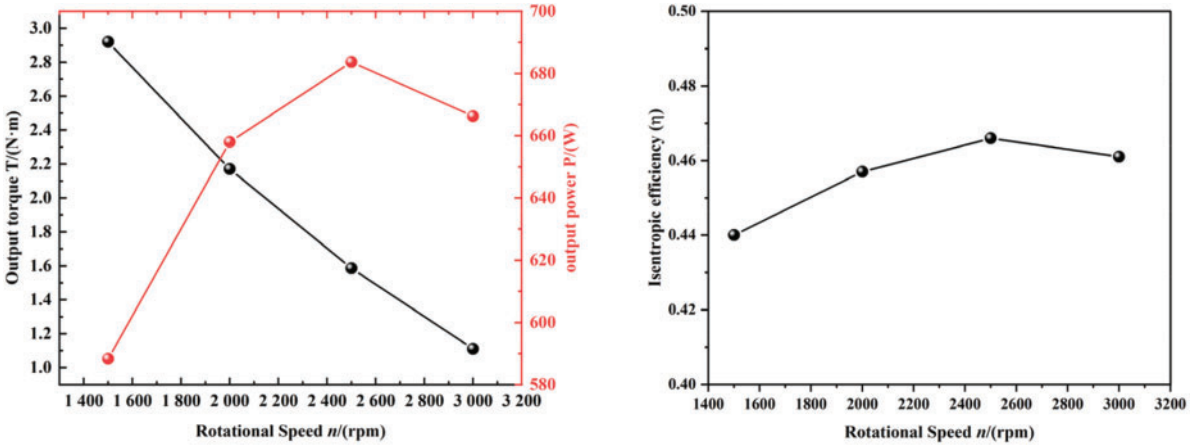

(a) Output torque and output power (b) Isentropic efficiency

Figure 9: Variation of scroll expander output performance with speed

4.4 Influence of Different Inlet Pressures on Expander Performance

As shown in Table 5, different inlet pressures were set to study the output performance of the expander at different inlet pressures. As can be seen from Fig. 10, when the expander speed and outlet pressure are kept fixed, the density of the work mass at the inlet will keep increasing with the pressure at a certain speed, while the speed will change less relative to the density, thus leading to an increase in mass flow. In one cycle, the average flow rate rises from 0.05603 to 0.07960 kg/s as the inlet pressure rises from 0.6 to 0.9 Mpa.

Table 5: Parameter settings for different pressures

Working conditions	Inlet pressure (Mpa)	Inlet temperature (K)	Outlet pressure (Mpa)	Rotational speed (rpm)
S1	0.6	373	0.1	2000
S2	0.7	373	0.1	2000
S3	0.8	373	0.1	2000
S4	0.9	373	0.1	2000

As shown in Fig. 11, when the speed of the expander and the outlet pressure remains constant, with the increasing air intake pressure the expander output torque and output power rise, this is due to the ideal working process of the scroll expander being the isentropic expansion process, when the

end-of-expansion pressure is certain, the increase in the inlet pressure will lead to an increase in the temperature difference between the import and export, thus increasing the output work. The isentropic efficiency of the scroll expander increases slowly with the increase in expander inlet pressure and increases by 6.61% when the expander inlet pressure increases from 0.6 to 0.9 Mpa.

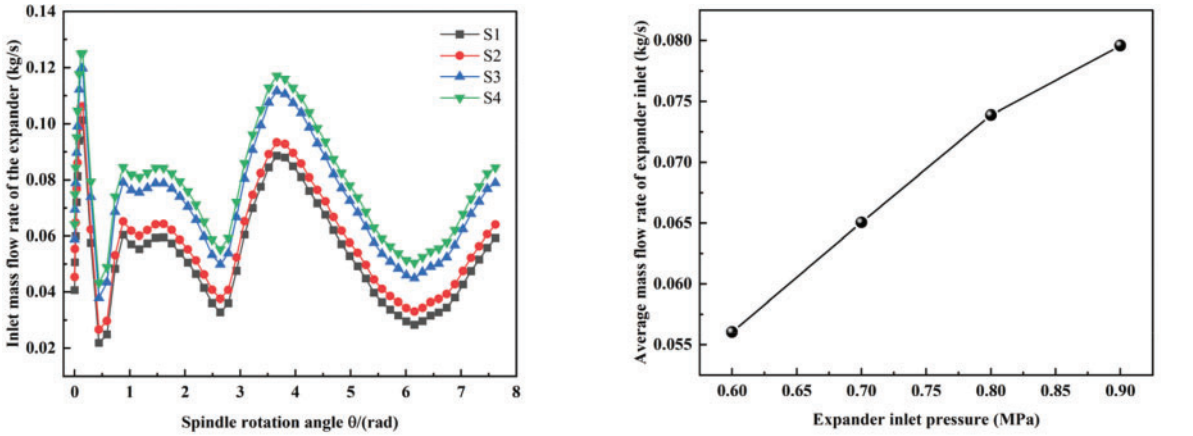

(a) Variation of inlet mass flow rate with the main shaft for scroll expanders at different pressures

(b) Scroll expander inlet average flow rate as a function of pressure

Figure 10: Flow rate *vs*. pressure at the inlet of a scroll expander

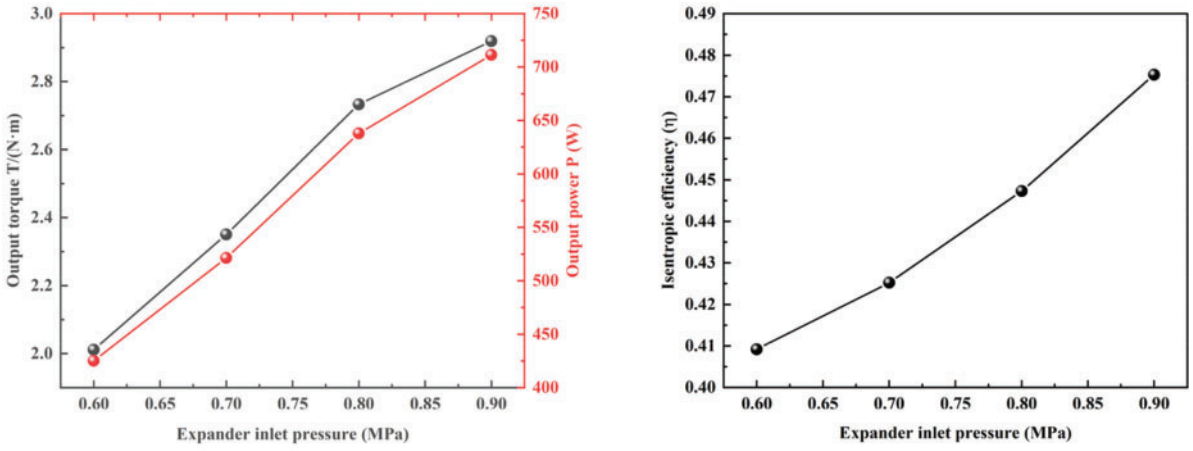

(a) Output torque and output power

(b) Isentropic efficiency

Figure 11: Variation of scroll expander output performance with pressure

5 Conclusion

This paper takes a variable base radius scroll expander as the object of study. Transient numerical simulations are carried out using dynamic mesh techniques and CFD methods to derive the internal flow field distribution pattern and transient output performance.

1. The variable base circle scroll expander has an asymmetric distribution of pressure, velocity, and temperature in the working cavity. The pressure gradually decreases from the suction cavity to the exhaust cavity, and there is tangential leakage at the scroll plate engagement, leading to a sharp increase in pressure loss and negative pressure phenomenon. There are varying degrees of swirling in the working cavity and large flow pulsation losses, which increase mechanical dissipation and lead to a gradual decrease in local temperature not from the suction cavity to the exhaust cavity.

2. While keeping the overall size of the expander unchanged, the output torque of the variable base circle scroll expander is increased by 0.046 N·m, the output power is increased by 9.634 W, and the isentropic efficiency is increased by 3.8% compared with that of the fixed base circle scroll expander. The combination of high sub-curves with fewer scroll turns in the same size results in a lower volumetric ratio, such that its output torque, output power, and efficiency are lower than that of a fixed-base circular scroll expander.

3. The circling scroll blocks the air intake as it spins, causing significant changes in the scroll expander's inlet flow throughout one cycle. The average mass flow rate rose by 0.03598 kg/s and the isentropic efficiency increased by 2.69% when the spindle speed was raised from 1500 to 3000 rpm. When the inlet pressure was grow from 0.6 to 0.9 Mpa, the average flow rate raised increased by 0.02357 kg/s, and the isentropic efficiency increased by 6.61%.

Acknowledgement: The authors would like to thank the research grant support from the Provincial Natural Science Foundation of Shandong and the Qingdao Emerging Industry Cultivation Program.

Funding Statement: This research was funded by the Provincial Natural Science Foundation of Shandong, Grant Number ZR2021ME233, ZR202103040075. This research was funded by the Qingdao Emerging Industry Cultivation Program, Grant Number 22-3-4-xxgg-7-gx.

Author Contributions: Conceptualization, Junying, W.; methodology, Junying, W.; software, Gang, L.; validation, Junying, W. and Gang, L.; formal analysis, Junying, W.; investigation, Junying, W.; resources, Junying, W.; data curation, Gang, L.; writing—original draft preparation, Gang, L.; writing—review and editing, Chenrui, Z.; visualization, Wenwen, C.; supervision, Jidai, W.; project administration, Junying, W.; funding acquisition, Junying, W. All authors have read and agreed to the published version of the manuscript.

Availability of Data and Materials: The datasets used or analysed during the current study are available from the corresponding author on reasonable request.

Conflicts of Interest: The authors declare that they have no conflicts of interest to report regarding the present study.

References

1. Olabi, A. G., Wilberforce, T., Ramadan, M., Abdelkareem, M. A., Alami, A. H. (2021). Compressed air energy storage systems: Components and operating parameters—A review. *Journal of Energy Storage, 34(3),* 24.
2. Wang, L. B., Bu, X. B., Li, H. S. (2020). Multi-objective optimization and off-design evaluation of organic rankine cycle (ORC) for low-grade waste heat recovery. *Energy, 203(15),* 117809.
3. Hu, S. Z., Yang, Z., Li, J., Duan, Y. Y. (2021). A review of multi-objective optimization in organic rankine cycle (ORC) system design. *Energies, 14(20),* 6492.

4. Wei, J., Hua, Q., Yuan, L., Li, G., Wang, J. et al. (2022). A review of the research status of scroll expander. *Proceedings of the Institution of Mechanical Engineers Part A-Journal of Power and Energy, 237(1),* 176–197.
5. Liu, Z., Wu, H. W., Lin, X., Song, P. P. (2019). Unsteady flows of a scroll expander under various types of expansion process. *Energy Storage Science and Technology, 8(6),* 1241–1246.
6. Peng, B., Li, Y., Zhao, S. (2018). Performance simulation for scroll expanders. *Zhongguo Jixie Gongcheng/China Mechanical Engineering, 29(8),* 965–970+978.
7. Yang, X. H., Pan, J. Z., Wang, J. D., Zhang, Z. Z. (2013). Numerical simulation research on the interior flow field of scroll expander. *Fluid Machinery, 41(2),* 15–18.
8. Liu, Z., Wu, W. H., Zhang, J., Kuang, Y. (2019). Numerical investigations on unsteady flow of a scroll expander forcompressed air energy storage. *Energy Storage Science and Technology, 8(2),* 357–364.
9. Emhardt, S., Song, P. P., Tian, G. H., Chew, J., Wei, M. S. (2018). CFD analysis of variable wall thickness scroll expander integrated into small scale ORC systems. *Energy Procedia, 158,* 2272–2277.
10. Song, P. P., Wei, M. S., Zhang, Y. J., Sun, L. W., Emhardt, S. et al. (2018). The impact of a bilateral symmetric discharge structure on the performance of a scroll expander for ORC power generation system. *Energy, 158,* 458–470.
11. Feng, Y. Q., Xu, J. W., He, Z. X., Hung, T. C., Shao, M. et al. (2022). Numerical simulation and optimal design of scroll expander applied in a small-scale organic rankine cycle. *Energy, 260(6),* 124981.
12. Sun, J., Peng, B., Zhu, B. G., Li, Y. H. (2023). Research on the performance characteristics of an oil-free scroll expander that is applied to a micro-scale compressed air energy storage system. *Journal of Energy Storage, 63,* 106896.
13. Wei, M. S., Song, P. P., Zhao, B., Shi, L., Wang, Z. X. et al. (2015). Unsteady flow in the suction process of a scroll expander for an ORC waste heat recovery system. *Applied Thermal Engineering, 78,* 460–470.
14. Song, P. P., Wei, M. S., Liu, Z., Zhao, B. (2015). Effects of suction port arrangements on a scroll expander for a small scale ORC system based on CFD approach. *Applied Energy, 150,* 274–285.
15. Qiang, J. G., Liu, Z. Q. (2006). End cross-section area calculation of EA-SAL modified scroll wrap. *Journal of Lanzhou University of Technology, 32(5),* 36–39.
16. Peng, B. (2019). Theoretical investigation on top profile modification of scroll expander. *Fluid Machinery, 47(6),* 15–19.
17. Peng, B. (2019). Study on geometry and leakage model of variable diameter involute scroll expander. *Machinery Design & Manufacture, 371(1),* 66–69+73.
18. Li, Z., Liu, Z., Wu, W. H., Xie, D. S., Qian, W. (2021). The transient flow field characteristics of tangential leakage inscroll compressor. *Energy Storage Science and Technology, 10(5),* 1579–1588.
19. Wu, Z., Feng, Z. G., Sun, Y. F. (2019). Simulation and analysis of internal flow field in scrollcompressor with circular involute profile. *Mechanical Science and Technology for Aerospace Engineering, 38(12),* 1840–1846.
20. Emhardt, S., Tian, G. H., Song, P. P., Chew, J., Wei, M. S. (2022). CFD analysis of the influence of variable wall thickness on the aerodynamic performance of small scale ORC scroll expanders. *Energy, 244,* 122586.
21. Chang, J. C., Chang, C. W., Hung, T. C., Lin, J. R., Huang, K. C. (2014). Experimental study and CFD approach for scroll type expander used in low-temperature organic rankine cycle. *Applied Thermal Engineering, 73(2),* 1444–1452.
22. Singh, S., Singh, A., Dasgupta, M. S. (2016). CFD modeling of a scroll work recovery expander for transcritical CO_2 refrigeration system. *International Conference on Recent Advancement in Air Conditioning and Refrigeration (RAAR), 109,* 146–152.
23. Cao, X. X., Shu, G. Q., Tian, H., Wang, M. T. (2021). Experimental study on output performance of scroll expander with designed lubrication system. *Thermal Power Generation, 50(6),* 91–97.
24. Cui, S., Wu, Z., Liu, L. C., Fang, X. Y., Gao, N. P. et al. (2019). Experimental investigation on performance of oil-free scroll expander. *Taiyangneng Xuebao/Acta Energiae Solaris Sinica, 40(1),* 30–37.

25. Yang, J. H., Sun, Z. Y., Liu, B. Q., Shi, J. Y., Chen, J. P. (2018). Parametric research on hermetic scroll expander integrated into vehicle organic rankine cycle power plant system. *Journal of Refrigeration, 39(4),* 106–110.
26. Li, L., Tao, L. R., Shen, L., Hu, Y. P., Li, Q. P. (2017). Improvement and experimental research on the performance of scroll expander using organic rankine cycle (ORC). *Chemical Industry and Engineering Progress, 36(5),* 1642–1648.
27. Chu, X. G., Zhang, C. H., Li, K., Kong, Y., Jin, Y. F. (2014). Improvement and performance experiment of a scroll expander. *Journal of Xi'an Jiaotong University, 48(1),* 37–41.
28. Wu, Z., Zhu, T., Gao, N. P., Cui, S., Pan, Y. et al. (2018). Experimental research on the performance of an oil lubricating scroll expander with air as the working medium. *Fluid Machinery, 46(6),* 5–9.
29. Sun, J., Peng, B., Zhu, B. G. (2022). Internal thermodynamic characteristics and performance test of new oil-free scroll compressor. *Jilin Daxue Xuebao (Gongxueban)/Journal of Jilin University (Engineering and Technology Edition), 52(12),* 2778–2787.
30. Liu, Z., Wei, M. S., Song, P. P., Emhardt, S., Tian, G. H. et al. (2018). The fluid-thermal-solid coupling analysis of a scroll expander used in an ORC waste heat recovery system. *Applied Thermal Engineering, 138,* 72–82.
31. Liu, Z., Wu, H. W., Song, P. P., Wei, M. S. (2020). Deformation analysis of a scroll expander for waste heat recovery of vehicle engine. *Neiranji Xuebao/Transactions of CSICE (Chinese Society for Internal Combustion Engines), 38(1),* 73–80.